Cerebral Cortex Advance Access published January 5, 2012

Cerebral Cortex
doi:10.1093/cercor/bhr360

Multimodal MRI Analysis of the Corpus Callosum Reveals White Matter Differences in Presymptomatic and Early Huntington's Disease

M. Di Paola[1,2], E. Luders[3], A. Cherubini[4,5], C. Sanchez-Castaneda[4,6], P. M. Thompson[3], A. W. Toga[3], C. Caltagirone[1,7], S. Orobello[8], F. Elifani[8], F. Squitieri[8] and U. Sabatini[4]

[1]Laboratory of Clinical and Behavioural Neurology, IRCCS Santa Lucia Foundation, 00179 Rome, Italy, [2]Department of Internal Medicine and Public Health, University of L'Aquila, 67010 L'Aquila—Coppito, Italy, [3]Laboratory of Neuro Imaging, Department of Neurology, UCLA School of Medicine, Los Angeles, CA 90095, USA, [4]Radiology Department, IRCCS Santa Lucia Foundation, 00179 Rome, Italy, [5]Neuroimaging Research Unit, Institute of Neurological Sciences, National Research Council, 88100 Catanzaro, Italy, [6]Department of Psychiatry and Clinical Psychobiology, University of Barcelona, Institut d'Investigacions Biomèdiques August Pi i Sunyer, 08036 Barcelona, Spain, [7]Neuroscience Department, University of Rome "Tor Vergata," 00133 Rome, Italy and [8]Centre for Neurogenetics and Rare Diseases, IRCCS Neuromed, 86077 Pozzilli, Italy

Address correspondence to Margherita Di Paola, IRCCS Santa Lucia Foundation, Via Ardeatina 306, 00179 Rome, Italy. Email: m.dipaola@hsantalucia.it.

Recent magnetic resonance imaging (MRI) studies suggest that abnormalities in Huntington's disease (HD) extend to white matter (WM) tracts in early HD and even in presymptomatic stages. Thus, changes of the corpus callosum (CC) may reflect various aspects of HD pathogenesis. We recruited 17 HD patients, 17 pre-HD subjects, and 34 healthy age-matched controls. Three-dimensional anatomical MRI and diffusion tensor images of the brain were acquired on a 3T scanner. Combining region-of-interest analyses, voxel-based morphometry, and tract-based spatial statistics, we investigated callosal thickness, WM density, fractional anisotropy, and radial and axial diffusivities. Compared with controls, pre-HD subjects showed reductions of the isthmus, likely due to myelin damage. Compared with pre-HD subjects, HD patients showed reductions of isthmus and body, with axonal damage confined to the body. Compared with controls, HD patients had significantly decreased callosal measures in extended regions across almost the entire CC. At this disease stage, both myelin and axonal damage are detectable. Supplementary multiple regression analyses revealed that WM reduction density in the isthmus as well as Disease Burden scores allowed to predict the "HD development" index. While callosal changes seem to proceed in a posterior-to-anterior direction as the diseases progresses, this observation requires validation in future longitudinal investigations.

Keywords: axonal demyelination, diffusion tensor imaging, region of interest, voxel-based morphometry, Wallerian degeneration, white matter changes

Introduction

Huntington's disease (HD) is a severe, dominantly transmitted neurodegenerative disease caused by an expansion CAG repeat mutation in the protein huntingtin (*HTT)* gene (Huntington's Disease Collaborative Research Group 1993). Its main neuropathological hallmark is the striatal degeneration (Vonsattel and DiFiglia 1998). However, the ubiquitous expression of the *HTT* gene mutation carries with it a cascade of toxic events that extend beyond the striatum to involve the cerebral cortex and white matter (WM) (Ciarmiello et al. 2006; for a review, see Esmaeilzadeh et al. 2011). The precise nature of such WM impairment is still unclear, and it is not known to what extent WM degeneration is part of the HD neuropathological profile. Changes in WM can develop as a consequence of a number of factors, including decreased number of axons, a consequence of cortical gray matter (GM) loss (Rosas et al. 2002, 2005; Kassubek et al. 2004; Douaud et al. 2006; Weaver et al. 2009), demyelination of axons (Mascalchi et al. 2004; Bartzokis et al. 2007; Rosas et al. 2010; Stoffers et al. 2010), or both.

The corpus callosum (CC) is the biggest WM tract in the human brain. Thus, analyzing callosal structure, in particular, will aid in understanding WM pathogenic processes associated with HD (i.e., axonal vs. myelin sheaths damage). Indeed, CC analysis has already shed light on many other neurological and psychiatric disorders (Tomaiuolo et al. 2004; Luders, Di Paola, et al. 2007; Kim et al. 2008; Kubicki et al. 2008; Di Paola, Luders, et al. 2010; Di Paola, Spalletta, et al. 2010).

First of all, changes in callosal subregions may mirror a degenerative process in brain areas other than the striatum because corticostriatal fibers are mainly conveyed by the external capsule (Schmahmann and Pandya 2006). Second, the CC interconnects homotopic brain corticocortical regions (Schmahmann and Pandya 2006), and according to the Wallerian degeneration hypothesis (Adams and Graham 1994), if a pathology is associated with changes in the cerebral cortex—as it happens in HD (Rosas et al. 2008)—then callosal fibers arising from those affected cortical areas should be affected too. Third, the CC contains fibers with different caliber and onset/completion of myelination across its structure. It contains generally larger and earlier myelinated fibers in posterior callosal subregions and smaller and late-myelinated fibers in anterior subregions (Aboitiz et al. 1992; Aboitiz and Montiel 2003). Thus, callosal fibers might be susceptible to damage at different time points during the course of the pathology.

Diffusion tensor imaging (DTI) is a noninvasive MR technique, which uses the local water diffusion in the brain tissues to study microstructural aspects of WM anatomy (Pierpaoli et al. 2001). Although the determinants of water diffusion in WM tissues are still not completely understood, there is general agreement that the diffusivity of water depends primarily on the presence of microscopic structural barriers in tissues, that can alter the random motion of water molecules. Membranes of cell bodies, axons, and myelin sheaths randomly impede the movement of water in the brain tissue, facilitating diffusion of water molecules preferentially along their main direction (Beaulieu 2002). When these structural barriers are damaged, the water is free to move in different directions. The computation of different DTI

parameters can give a cue on what is likely going on in the brain tissues. Briefly, fractional anisotropy (FA) is related to the degree to which water diffusion is directionally constrained, and a decreased FA indicates a loss of water directionality likely due to a damage in structural organization of the tissue (Schulte et al. 2005). Axial diffusivity (DA) is related to the tendency of water to diffuse in a direction parallel to the WM fibers, and an increased DA is related to WM axonal atrophy likely associated with Wallerian degeneration. Radial diffusivity (DR) expresses diffusivity in the direction perpendicular to the WM fibers, and an increased DR is related to WM fiber damage that is more likely associated with breakdown of the myelin sheaths (Song et al. 2002; Kim et al. 2006).

The assumption, arising from experiments using animal models (Choi et al. 2005; Sun et al. 2005), is that significantly reduced DR in WM, without differences in DA, might indicate specifically compromised myelin integrity in the absence of axonal structural irregularities. Thus, taken together, these different diffusivity measurements should help us to understand the different mechanisms underlying microstructural callosal changes (i.e., axonal vs. myelin sheaths damage). Indeed, the simultaneous use of different DTI parameters (FA, DR, and DA) has already been proven to be helpful when studying the intrinsic differences of callosal WM changes and their relationship to AD (Di Paola, Di Iulio, et al. 2010).

Bartzokis's hypothesis on demyelination in HD suggests that WM breakdown affects early-myelinized CC fibers (Bartzokis et al. 2007). Therefore, we would expect the main callosal changes occurring early in posterior subregions (i.e., within the splenium and isthmus). Even so, very few studies have focused on callosal changes in HD (Rosas et al. 2010). Previous macrostructural studies in symptomatic subjects have reported atrophy within the splenium, genu, and portions of the callosal body (Hobbs et al. 2010) or a reduced thickness across the entire CC (Rosas et al. 2010). They did not find any callosal change in pre-HD subjects, suggesting that the total number of fibers is not reduced in the early phase of HD (Hobbs et al. 2010; Rosas et al. 2010). Microstructural studies applying DTI reported reductions in FA in HD compared with matched control subjects in the genu, body, and splenium (Rosas et al. 2006). The same authors, in a second study (Rosas et al. 2010), found significantly lower FA and increased DR and DA across the entire CC in the HD group, indicating that the changes in callosal fibers are due to both axonal damage and demyelination. Moreover, pre-HD subjects showed lower FA in the body of the CC relative to matched controls (Rosas et al. 2006). The same group later observed significant reductions in FA across the CC in the pre-HD, with higher DR in genu, body, and splenium and no difference in DA (Rosas et al. 2010). Similarly, Stoffers et al. (2010) reported lower FA and increased DR in pre-HD in the genu, body, and isthmus, with no differences in DA. Taken together, these data suggest a loss of integrity in callosal fibers (microstructural changes) in the pre-HD. However, the loss seems to spare parts of the callosal body and appears to be mainly characterized by myelin sheath damage (as indicated by the observed differences in DR but not DA). The scenario is more complex in HD, where the whole CC is involved, and both axonal damage and demyelination are implicated.

In this study, we examined potential CC changes in a cohort of subjects at the pre- (n = 17) and first stages (n = 17) of HD compared with control subjects. The main aims of our study were to elucidate if WM changes (axonal degeneration and/or demyelination processes) occur in the CC; and to analyze whether such changes might represent a source for a possible biomarker of HD. For this purpose, we used a multimodal imaging approach, combining 3 well–validated macrostructural and microstructural analysis techniques, including 1) computational mesh-based methods to map callosal thickness with high spatial resolution; 2) voxel-based morphometry (VBM) to map callosal WM density, and 3) DTI using tract-based spatial statistics (TBSS) to investigate microstructural differences in callosal WM via calculating FA, DA, and DR.

Materials and Methods

Subjects

All HD subjects (n = 34) underwent a genetic test (abnormal CAG repeats > 40) and were examined clinically by the same neurologist with expertise in HD. Seventeen pre-HD subjects and 17 patients in the early disease stages (I and II) were enrolled in the study. All individuals were assessed using the Unified Huntington's Disease Rating Scale (UHDRS) motor, cognitive, behavioral, and functional subscales (Huntington Study Group 1996). Each section is composed by a multiitem subscale. The motor section measures several body districts, including eye movements, limb coordination tongue impersistence, movement disorders, such as rigidity, bradykenisia, dystonia, chorea, and gait disturbances. The cognitive scale assays mainly the executive function. The behavioral section investigates the presence of depression, aggressivity, obsessions/compulsions, delusion/hallucinations, and apathy. The functional assessments include the HD functional capacity scale (HDFCS), the independence scale, and a checklist of common daily tasks. All of these 3 scales investigate mainly the subject's independence in the daily activities. The HDFCS is reported as the total functional capacity (TFC) score (range 0–13) and is the only functional subscale with established psychometric properties including interrater reliability and validity, based on radiographic measures of disease progression. Thus, the TFC score is used worldwide to determine HD stage. In the independence scale, the investigator indicates if the patient can perform the task evaluating the level of the subject's independence (range 10–100). The checklist (functional assessment) is summed by giving a score of 1 to all "yes" answers (range 0–25).

Pre-HD subjects included asymptomatic (total motor score of <5 in the UHDRS) and individuals with "soft signs" (suspicious clinical features insufficient to perform diagnosis of HD) (Paulsen et al. 2001). The patients' age at disease onset was established based on the first neurological manifestations (Squitieri et al. 2003). A prediction of the number of years to diagnosis were calculated based on a survival analysis formula described by Langbehn et al. (2004). Furthermore, in an attempt to estimate the progression of the pathological process since the presymptomatic stage, we calculated an "HD development" index combining the predicted years to onset for pre-HD subjects and disease duration (years from onset) for patients. In other words, the index is calculated according to the number of years from a given pre-HD subject's age to the predicted age at onset (on the basis of the CAG mutation size) and according to the number of years from the real patient's age at onset to the patient's age at the last clinical exam (i.e., duration of HD). As a measure of disease progression, the HD development has the advantage of including both pre-HD and HD groups on the same scale. The subjects near age at onset and at the first HD stage have been followed-up for many years, thus allowing a prospective interpretation of age at onset. Only for a few more advanced symptomatic cases in the current study, age at onset was calculated by careful retrospective analysis with the help of the patients' relatives.

Disease Burden index was measured according to the already described formula (age × [CAG-35.5]), where CAG is the number of CAG repeats (Penney et al. 1997). Thirty-four individually age- and sex-matched healthy subjects were recruited from the community. Patients in the advanced stages of disease (Stages III and IV) and/or with traumatic brain injury or magnetic resonance imaging (MRI) focal lesions were excluded. Demographic and clinical characteristics of the sample are shown in Table 1. The local ethics committee

Table 1
Sociodemographic and clinical characteristics of patients and control subject

	Pre-HD (n = 17)	Pre-HD CTL (n = 17)	HD (n = 17)	HD CTL (n = 17)	Fisher's exact test; F or T	df	P
Characteristics							
Gender male (n, %)	12, 70.6%	12, 70.6%	10, 58.8%	10, 58.8%	1.089		0.837
Age in years (mean ± SD)	39.1 ± 7.2	39.1 ± 7.4	50.12 ± 12.6	50.53 ± 12.9	6.647	3	0.017[a,††]; 0.012[b,††]
CAG repetition length	44.1 ± 1.7	NA	45.1 ± 4.1	NA	−0.926	32	0.362
Disease duration in years (range)			0–13				
Estimated years to onset (range)	−25 to 0						
HD development in years (mean ± SD)	−8.65 ± 6.76		5.83 ± 4.49				
MMSE	28.1 ± 1.8	NA	25.5 ± 3.7	NA	2.549	29	0.016[a]
UHDRS motor	8.3 ± 7.1	NA	38.4 ± 14.3	NA	−7.563	31	0.000[a]
UHDRS cognitive	254.1 ± 45.5	NA	142.5 ± 51.1	NA	6.608	31	0.000[a]
UHDRS behavioral	7.3 ± 6.9	NA	19.2 ± 9.7	NA	−4.070	31	0.000[a]
UHDRS functional	25 ± 0	NA	18.1 ± 4.6	NA	6.140	32	0.000[c]
TFC	13 ± 0	NA	8.4 ± 1.8	NA	10.482	32	0.000[c]
Independence scale	99.7 ± 1.2	NA	78.5 ± 10.9	NA	7.988	32	0.000[c]
Disease Burden	331.8 ± 54.0	NA	438.1 ± 96.2	NA	−3.969	32	0.000[a]

Note: Pre-HD, gene-positive, without motor symptoms; Pre-HD CTL, control subjects for Pre-HD; HD CTL, control subjects for HD; SD, standard deviation; df, degrees of freedom; CAG, trinucleotide repeat number; MMSE, Mini-Mental State Evaluation; NA, not available; ††T-student. Bonferroni correction.
[a]Pre-HD < HD higher scores mean greater impairment.
[b]Pre-HD CTL < HD CTL.
[c]Pre-HD > HD higher scores mean lesser impairment.

approved the study; written informed consent was obtained from all participants.

MRI Data Acquisition

All MRI data were acquired on a 3T Allegra MRI system (Siemens, Erlangen, Germany) using a birdcage head coil. Scans were collected in a single session, with the following pulse sequences: 1) proton density and T_2-weighted double turbo spin echo (SE) acquired in transverse planes (time repetition [TR]: 4500 ms, time echo [TE]: 12 ms, time to inversion [TI]: 112 ms, field of view [FOV]: 230 × 172 mm, matrix: 320 × 240, slice thickness: 5 mm, number of slices: 24); 2) fluid-attenuated inversion recovery in the same planes as the SE sequence (TR/TE/TI: 8500/109/2000 ms; FOV: 230 × 168 mm, matrix: 256 × 256, slice thickness: 5 mm, number of slices: 24); 3) T_1-weighted 3D images, with partitions acquired in the sagittal plane, using a modified driven equilibrium Fourier transform (Deichmann et al. 2004) sequence (TE/TR/TI: 2.4/7.92/910 ms, flip angle: 15°, 1 mm^3 isotropic voxels); and 4) diffusion-weighted volumes were also acquired using SE echo-planar imaging (TE/TR: 89/8500 ms, bandwidth: 2126 Hz/voxel, matrix: 128 × 128, 80 axial slices, voxel size: 1.8 × 1.8 × 1.8 mm) with 30 isotropically distributed orientations for the diffusion sensitizing gradients at a b value of 1000 s/mm^2 and 6 b = 0 images. Scanning was repeated 3 times to increase the signal-to-noise ratio.

Images were visually inspected for gross anatomical abnormalities by 2 experienced observers (a neuropsychologist expert in neuroimaging and a neuroradiologist), blind to participant identities.

Callosal Thickness Analysis (Region-of-Interest Approach)

Radio frequency bias-field corrections were applied to all images to reduce intensity drifts due to magnetic field inhomogeneities (Sled et al. 1998). Images were linearly registered to the Montreal Neurological Institute (MNI) 305 template using 9-parameter transformations to adjust for brain orientation, translation, and size.

Finally, regional callosal thickness was estimated in a 3-step approach detailed elsewhere (Luders et al. 2006; Luders, Narr, et al. 2007). First, upper and lower callosal boundaries were manually outlined in the midsagittal section of each brain (Step I). More specifically, using the bias-corrected and -scaled images, an expert rater (M.D.P.) choose, for each brain image, the most midsagittal MRI slice, where the septum pellucidum and the falx were simultaneously visible. The callosal boundaries were, dorsally and rostrally, the pericallosal sulcus, and ventrally, the III ventricle, and the cisterna superior. Subsequently, the spatial average from 100 equidistant surface points representing the upper and lower boundaries was calculated, and a new midline segment (also consisting of 100 equidistant points) was created (Step II). Distances between 100 corresponding surface points from this new midline to upper/lower boundaries were quantified (Step III). Using the callosal distance values, we applied independent sample t-tests to compare the 3 groups (pre-HD subjects vs. controls, HD patients vs. controls, and pre-HD subjects vs. HD patients).

Callosal WM Density Analysis (VBM Approach)

Images were processed and analyzed using VBM (Ashburner and Friston 2000; Good et al. 2001) in the statistical parametric mapping framework (SPM5, Wellcome Department of Imaging Neuroscience, University College London, UK). To improve image registration, images were first manually reoriented to approximate the orientation to that of the ICBM-152 default SPM5 template. Each volume was segmented into WM partitions. Then, the Diffeomorphic Anatomical Registration Through Exponential Lie Algebra (DARTEL) toolbox was applied to the WM partitions. This allows a high-dimensional normalization, preserving brain topology. Template creation is incorporated into the algorithm and a new template based on the entire sample is recreated at the end of each iteration. This technique improves the realignment of small inner structures (Yassa and Stark 2009). Then, we used a script to transform DARTEL template and images to MNI space (D MacLaren, personal communication). Finally, WM partitions (unmodulated data) were smoothed using a Gaussian kernel of 8 mm full-width at half-maximum, and entered into subsequent statistical analyses.

We applied independent sample t-tests at each voxel to compare groups (pre-HD subjects vs. controls, HD patients vs. controls, and pre-HD subjects vs. HD patients). Statistical maps were corrected for multiple comparisons by controlling the false discovery rate (FDR) at 5%. Significant findings were mapped onto the ICBM-152 default SPM5 template.

Callosal FA, DA, and DR Analysis (TBSS Approach)

Diffusion-weighted images were processed with FMRIB's Software Library (FSL 4.1 www.fmrib.ox.ac.uk/fsl/). Image distortions, induced by eddy currents and head motion, in the DTI data, were corrected by applying a full affine alignment of each image to the mean no diffusion-weighted image. After corrections, DTI data were averaged and concatenated into 31 (1 B0 + 30 B1000) volumes. A diffusion tensor model was fitted at each voxel, generating FA, DA, and DR maps. DR was defined as the average of the second and third eigenvalues of the diffusion tensor, while DA corresponded to the first eigenvalue.

We used TBSS (Smith et al. 2006), version 1.2, which is part of the FSL software package, for the postprocessing and analysis of the multi-subject DTI data. First, a target image was calculated using all subjects' FA maps; then, all subjects' FA maps were nonlinearly aligned to the target FA image. The mean FA image was subsequently thinned to create a mean FA skeleton by using a local search for each voxel in the

direction perpendicular to the tracts. A threshold FA value of 0.2 was then applied to exclude voxels that were primarily GM or CSF. Each subject's aligned FA data was then projected onto this skeleton using a search algorithm. The same transformations derived for the FA maps were applied to the DA and DR maps.

To test for localized differences across groups (pre-HD subjects vs. controls, HD patients vs. controls, and pre-HD subjects vs. HD patients), voxelwise statistics were performed for each point on the common FA skeleton. A permutation-based approach (Nichols and Holmes 2002) that accounts for "family wise errors" was used to control for multiple comparisons. Specifically, permutation-based inference on cluster size ($t > 1$, $P < 0.05$) was used to test whether FA was reduced in HD compared with control and pre-HD subjects and whether DR and DA were significantly increased. The significant voxels from 3 midsagittal slices (MNI, $x = -1; 0; +1$) were projected onto a 2D sagittal plane.

Correlation between Callosal Measures and Whole-Brain GM

To further explore the mechanisms underlying the callosal modifications, we investigated how callosal differences in pre-HD and HD group were related to whole-brain GM (obtained with the VBM processing).

Briefly, as shown in Figure 1, in the main macrostructural analyses (thickness and VBM analyses), we found that the isthmus was thinner in pre-HD compared with control subjects (Panels *A* and *D*). In the same region, at a microstructural level, we also found decreased FA, increased DR, and no changes in DA (in the DTI analysis; Panels *G*, *M*, and *J*). In contrast, in HD patients compared with control subjects, we found a significant macrostructural and microstructural difference across almost all of the CC (Panels *C*, *F*, *I*, *L*, and *O*). However, we found a peculiar feature in the microstructural callosal differences in HD patients: that is, the only callosal subregions associated with an increased DA were the isthmus and the body (Panels *K* and *L*).

Based on the hypothesis that atrophy of the isthmus in pre-HD may be due to myelin breakdown (DR changes and not DA changes), we expected to not find any correlation between isthmus and cortical GM measures in this group. On the other hand, based on the hypothesis that atrophy of the isthmus and body in HD patients may be due to both myelin breakdown (changes in DR) and Wallerian degeneration (changes in DA), we expected to find a correlation between measures of the isthmus, body, and cortical GM.

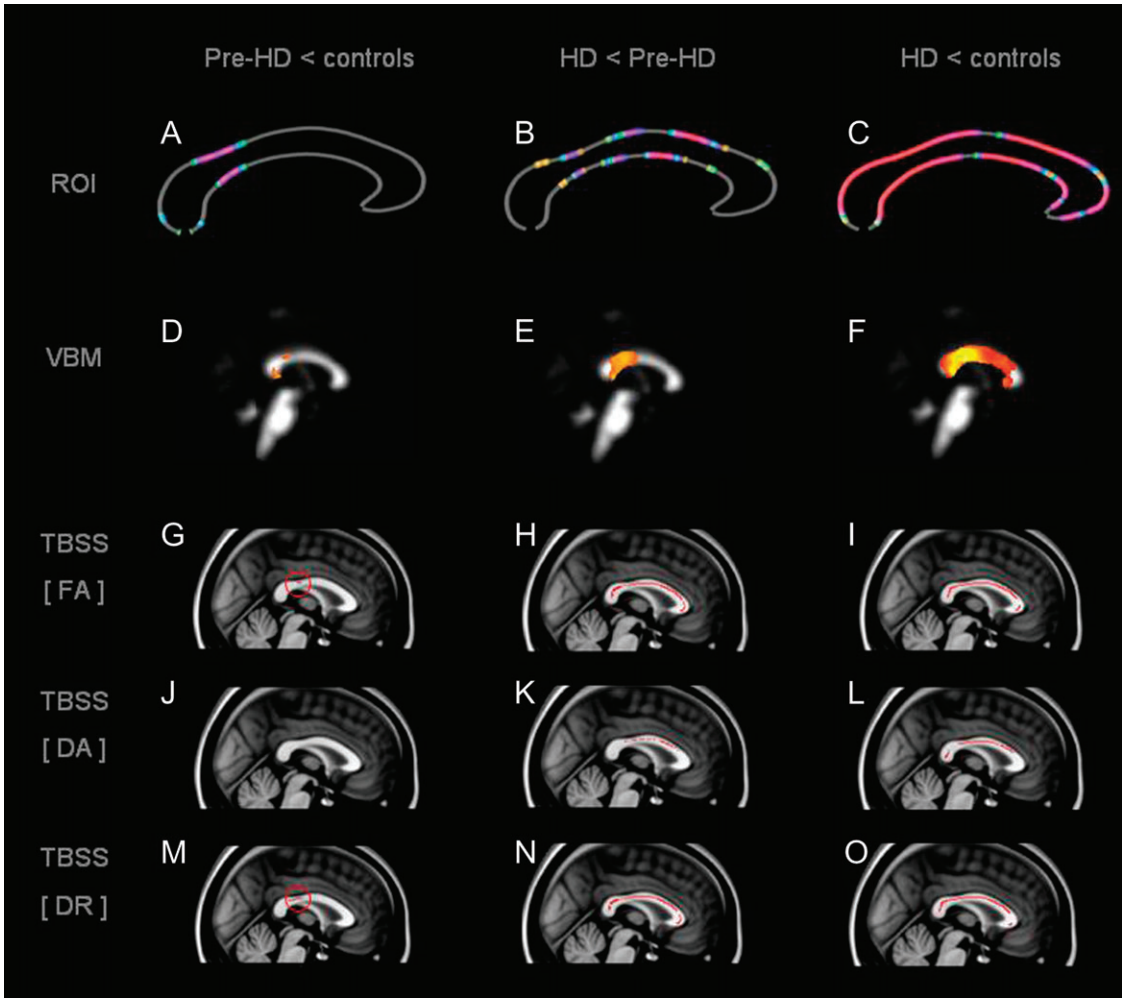

Figure 1. Microstructural and macrostructural changes in pre-HD subjects and HD patients. The left panels display the results of the comparison between pre-HD versus controls. The central panels display the results of the comparison between pre-HD versus HD. The right panels display the results of the comparison between HD versus controls. The top panels show the results of the callosal thickness analysis. The middle panels show the results of the VBM analysis. The bottom panels show the results of the DTI analysis. Compared with controls, pre-HD patients show a reduced callosal thickness in the isthmus (Panel *A*); a reduced WM density in the isthmus and splenium (Panel *D*); a reduced FA in the isthmus (Panel *G*); no changes in DA (Panel *J*); increased DR in the isthmus (Panel *M*). Compared with pre-HD, HD patients show a reduced thickness mainly in the body (Panel *B*); a reduced WM density in the splenium, isthmus, and rostrally in the rostrum (Panel *E*); reduced FA and DR across the entire CC (Panels *H* and *N*) as well as an increased DA in the body (Panel *K*). Compared with controls, HD patients show a reduced thickness almost across the entire CC (Panel *C*); a reduced WM density in the splenium, isthmus, and body (Panel *F*); reduced FA and DR in all the CC (Panels *I* and *O*) as well as an increased DA in the isthmus and body (Panel *L*).

Thus, we correlated the isthmus measures for the pre-HD group with the whole GM maps, and the isthmus and the body for the HD group with the whole GM maps.

To calculate the average isthmus callosal WM density for the pre-HD subjects, we extracted and averaged the intensity values of the posterior CC region (corresponding to the cluster where we found a difference between the pre-HD and the control group with the VBM approach; see Fig. 1, Panel *D*). To calculate the average isthmus and the body callosal WM density of HD patients, we extracted and averaged the intensity values of the posterior CC region (corresponding to the cluster where we found the difference in HD and the control group with the VBM approach; see Fig. 1, Panel *E*).

Then, we ran 2 multiple regression analyses in SPM5. In the first one, we entered into the matrix the whole GM maps of pre-HD subjects and the isthmus values. In the second one, we entered the isthmus and the body values as predictors and the whole-brain GM maps of the HD subjects.

Given the lack of published data linking callosal and cortical GM density features in pre-HD and HD, we performed an exploratory investigation, using an uncorrected significance threshold (to reduce the risk of missing true-positive results).

Multiple Linear Regression Analyses

We also wanted to determine whether there was one or more predictors of the HD development index (considered as dependent variables) among the sociodemographic, clinical, genetic, neuropsychological, and neuroimaging data. To do this, we conducted a stepwise multiple regression analysis. Independent variables included in the stepwise regression models were preselected by performing correlation analyses between variables (scores were previously transformed in *Z* scores), to determine the significance of the correlations (see Table 2). That is, for the stepwise multiple regression analysis, only variables with a $P < 0.0033$ ($P = 0.05/15$, Bonferroni correction for multiple comparisons) in the preselection correlation analyses, were included as independent variables. Statistical analyses were performed with SPSS Software.

Results

Demographic and Clinical Characteristics

The pre-HD subjects and HD patients did not differ from their respective control groups in age or sex (see Table 1). There were also no differences in sex or CAG repetition length between pre-HD subject and HD patients; however, as might be expected, these groups differed in age. Thus, we entered age as a covariate in each statistical analysis that compared pre-HD subject versus HD patients. As expected, HD patients had significantly poorer performances with respect to all measures assessed by the UHDRS (see Table 1), and also a significantly higher score at Disease Burden (see Table 1).

Table 2
Sociodemographic, clinical, genetic, and neuroimaging neuropsychological and neuroimaging correlates of "HD development"

Characteristics	HD development	
	r	*P* value
Educational level	−0.270	0.061
CAG repetition length	0.065	0.357
MMSE	0.133	0.227
UHDRS motor*	−0.088	0.311
UHDRS cognitive	**0.557**	**0.000**[a,b]
UHDRS behavioral	−0.174	0.163
UHDRS functional	**−0.704**	**0.000**[a,b]
TFC	**−0.805**	**0.000**[a,b]
Independence scale	**−0.781**	**0.000**[a,b]
Disease Burden	**0.418**	**0.007**[a,b]
WM thickness body	**−0.523**	**0.001**[a,b]
WM density isthmus	**−0.830**	**0.000**[a,b]
FA all CC	**−0.784**	**0.000**[a,b]
DA body	**0.682**	**0.000**[a,b]
DR all CC	**0.759**	**0.000**[a,b]

Note: CAG, trinucleotide repeat number; MMSE, Mini-Mental State Evaluation.
[a]Significant at the uncorrected statistical level ($P < 0.05$).
[b]Significant at the corrected statistical level ($P < 0.033$), evidenced in bold.
*Conducting a correlation analysis between "HD development" index and UHDRS motor scale for HD patients alone revealed a significant-positive correlation ($r = 0.492$, $P = 0.45$).

Callosal Thickness Analysis (Region-of-Interest Approach)

As shown in Figure 1 (Panel *A*), when pre-HD patients were compared with control subjects, we detected a significantly smaller callosal thickness within the isthmus. When pre-HD subjects were compared with HD patients (Panel *B*), the CC in HD patients was not only thinner within the isthmus but also more anteriorly as well, involving the callosal body as far as to the border between the anterior body and the anterior third. When HD patients were compared with control subjects, (Panel *C*), we found a significantly reduced callosal thickness across almost the entire callosal surface. Control subjects did not show any region where callosal thickness was reduced relative to either patient group (results not shown).

Callosal WM Density Analysis (VBM Approach)

As further shown in Figure 1, when pre-HD subjects were compared with control subjects (Panel *D*), we found some regions with WM density reductions within the isthmus, but this result did not survive correction for multiple comparisons. When pre-HD subjects were compared with HD patients (Panel *E*), we observed a reduced callosal WM density in an area involving the splenium and isthmus ($Z = 4.64$, FDR-corrected $P = 0.015$) and within the rostrum ($Z = 4.00$, FDR-corrected $P = 0.015$). When HD patients were compared with control subjects (Panel *F*), we found a significantly reduced WM density across almost the entire posterior callosal surface (splenium and isthmus) as well as within parts of the callosal body ($Z = 6.03$, FDR-corrected $P < 0.001$). Control subjects did not show any region where WM density was reduced when compared with either of the 2 patient groups (results not shown).

Callosal FA Analysis (TBSS Approach)

As shown in Figure 1, the spatial distribution of differences ($P < 0.05$) between pre-HD and control subjects in DTI parameters were as follows: 1) FA was lower in the isthmus of the CC in pre-HD subjects (Panel *G*); 2) there was no significant difference in DA between groups (Panel *J*); and 3) DR was greater in the isthmus of the CC in pre-HD subjects (Panel *M*).

The spatial distribution of differences ($P < 0.05$) between pre-HD subjects and HD patients in DTI parameters was as follows: 1) FA was lower in all CC regions in HD patients (Panel *H*); 2) DA was higher within the callosal body in HD patients (Panel *K*); and 3) DR was greater in all CC regions in HD patients (Panel *N*).

The spatial distribution of differences ($P < 0.05$) between HD patients and control subjects in DTI parameters was as follows: 1) FA was lower in all CC regions in HD patients (Panel *I*); 2) DA was higher within the isthmus and callosal body in HD patients (Panel *L*); and 3) DR was higher in all CC regions in HD patients (Panel *O*).

Correlation between Callosal Measures and Whole-Brain GM

We found that measures derived from the isthmus in pre-HD subjects did not predict GM changes in any cortical GM regions. Even so, in HD patients, we found that measures derived from the isthmus did predict GM changes with right precuneus (BA 7), and measures of the callosal body correlated positively with the left medial frontal gyrus (BA 6).

Multiple Linear Regression Analyses

Univariate correlations among sociodemographic, clinical, genetic, neuropsychological neuroimaging variables, and the HD development index are shown in Table 2. Preselection analyses revealed that HD development was significantly correlated (either positively or negatively) with a number of variables (summarized in Table 2). However, subsequent stepwise multiple regression analyses indicated that none of the other predictors contributed significantly after 1) WM density in the isthmus and 2) Disease Burden scores were entered into the regression analysis. The resulting regression model was significant ($F = 80.2$, degrees of freedom = 2,31, $P < 0.001$) and explained 83.8% of the overall variance of the HD development index. More specifically, a lower value of WM density in the isthmus and a higher score at Disease Burden predicted a higher HD development index (Table 3).

Discussion

In pre-HD subjects, we found that the isthmus was the most affected CC subregion. This agrees with observations by Rosas et al. (2010), who investigated the magnitude of thinning of each callosal segment as a percentage. They also observed the isthmus to be severely affected. Similarly, our DTI analysis detected FA and DR differences only in the isthmus of pre-HD subjects. In agreement with other studies (Rosas et al. 2010), we did not find any significant DA difference in pre-HD subjects confirming the assumption of myelin damage in these pre-symptomatic stages. This seems to be further substantiated by the lack of any observed correlation between isthmus attributes and cortical GM density measures.

Of note, the lack of correlation between isthmus measures and cortical GM density in pre-HD is not imputable to a lack of abnormality in GM density in this group of patients. A VBM-DARTEL analysis conducted on GM maps (pre-HD vs. HC and HD vs. HC) (data not shown) revealed a significant (FDR = 0.05) cortical GM reduction in both patients group. When compared with HC, pre-HD subjects presented a volume reduction involving precentral, superior, and middle frontal gyrus (approximating Brodmann areas [BAs] 4, 6, and 8) as well as occipital gyrus (approximating BA 19).

In HD patients, the whole CC was significantly thinner and also showed a diminished WM density compared with control subjects, which agrees with outcomes of previous studies (Hobbs et al. 2010; Rosas et al. 2010). FA and DR were also significantly different in all CC regions compared with control subjects, and increased DA was evident only within the isthmus and body. These findings suggest that both myelin breakdown (reflected by the increased DR) and axonal damage (reflected by the increased DA) may affect the callosal WM when HD is fully manifested. Our results suggest that axonal damage within the isthmus and body might be mirrored by cortical GM abnormalities, as indicated by the positive correlations between callosal attributes and cortical GM measures. Moreover, the VBM analysis revealed a cerebral GM reduction in HD patients within the sensorimotor cortex (BAs 2 and 1), precentral gyrus (BA 6), and occipital cortex (BAs 18 and 19).

Comparisons between pre-HD subjects and HD patients further suggest that CC changes are temporally and spatially well defined. They seem to be detectable within the isthmus in pre-HD subjects and proceed in a posterior-to-anterior direction, eventually involving both the isthmus and the body in HD patients. Although we did not find any correlations between measures of the CC and cerebral cortex in pre-HD, previous studies on pre-HD subjects (Rosas et al. 2003, 2005) revealed a posterior-to-anterior degeneration pattern with respect to the cerebral cortex.

The results of comparing pre-HD and HD subjects confirm that the difference within the isthmus in pre-HD is most likely caused by specific damage to myelin sheaths (i.e., we observed changes in DR but no changes in DA). In later stages, these alterations seem to be driven by both myelin and axonal damage (i.e., we observed changes in both DR and DA in HD patients).

Table 3
Stepwise multiple regression analysis: predictors of "HD development"

Variables	Step 1[a]	Step 2[a]
WM density—isthmus Standard coefficient and (*t* value)	**−0.830 (−8.410)**	**−0.815 (−11.268)**
Disease Burden Standard coefficient and (*t* value)	0.387 (5.349)	**0.387 (5.349)**
UHDRS cognitive Standard coefficient and (*t* value)	−0.028 (−0.212)	0.063 (0.644)
UHDRS functional Standard coefficient and (*t* value)	−0.105 (−0.631)	0.009 (0.072)
TFC Standard coefficient and (*t* value)	−0.336 (−1.697)	−0.139 (−0.897)
Independence scale Standard coefficient and (*t* value)	−0.297 (−1.726)	−0.152 (−1.150)
Callosal thickness—callosal body Standard coefficient and (*t* value)	0.184 (1.279)	0.076 (0.692)
FA—whole CC Standard coefficient and (*t* value)	−0.272 (−1.437)	−0.098 (−0.671)
DA—callosal body Standard coefficient and (*t* value)	0.060 (0.366)	0.075 (0.626)
DR—whole CC Standard coefficient and (*t* value)	0.190 (1.008)	0.084 (0.598)
r^2	**0.688**	**0.838**
P	**<0.000**	**<0.000**

Note: CAG, trinucleotide repeat number; MMSE, Mini-Mental State Evaluation.
[a]Standard coefficient and (*t* value).

Possible Underlying Mechanisms

While corticostriatal dysfunction has been historically considered the main mechanism underlying the neuropathology in HD (Walker 2007), this mechanism by itself cannot totally explain callosal alterations. Wallerian degeneration or demyelination may also be involved. More specifically, the "demyelination hypothesis" of HD assumes that early and heavily myelinated fibers, such those in the isthmus, are more susceptible to myelin breakdown (Bartzokis et al. 2007). Demyelination is consistent with neuropathologic findings in pre-HD, which show increased density of oligodendrocytes, which may be a developmental effect of the HD gene expansion (Gomez-Tortosa et al. 2001). Indeed, the breakdown of early and heavily myelinated fibers is consistent with an

increased density of oligodendrocytes attempting to repair myelin damage. This repair process increases the iron levels caused by the increased numbers of oligodendrocytes, which are the brain cell type with the highest ferritin content (Bartzokis et al. 2007). Iron accumulation is hypothesized to cause further damage (such as oxidative stress) and, indeed, most hypotheses concerning HD pathogenesis include a role for oxidative damage (Beal 1996). However, the relationship between callosal WM demyelination and iron accumulation in HD needs further confirmation.

The "Wallerian hypothesis," on the other hand, assumes that callosal axonal damage is a consequence of the death of projecting pyramidal cells in layer III of the neocortex and could reflect the pattern of neocortical neurodegeneration (Leys et al. 1991). Based on Wallerian degeneration, we expected that the CC subregions modifications in HD should reflect changes in the cerebral cortex connected through those callosal areas. In our HD patients, we found that differences in the isthmus and body, correlated with a reduced cerebral GM density, supporting the Wallerian degeneration hypothesis.

Innovation and Future Research

One innovative aspect of this study is that we used several DTI measures (FA, DR, and DA) to study callosal WM differences (Song et al. 2002, 2003; Choi et al. 2005; Sun et al. 2005) as well as correlations between CC measures and cortical GM measures. This approach was helpful in disentangling different possible mechanisms affecting callosal WM in presymptomatic and early HD.

Recently, a third hypothesis has been proposed to explain WM changes in HD. This theory suggests that abnormal brain development may contribute to the pathogenesis of HD, as precursor to the more global neurodegeneration process (Nopoulos et al. 2010). According to this theory, our results within the isthmus in pre-HD may reflect a slowing in brain development, after an initial normal growth that spares the splenium. Further studies that will follow young pre-HD subjects longitudinally may help in addressing this possibility.

Our multivariate analysis shows that the WM density of the callosal isthmus, together with the Disease Burden score (Penney et al. 1997), is able to explain most of the variance in HD development. The role of the Disease Burden as measure of disease severity in HD has been previously demonstrated (Bechtel et al. 2010). In contrast, considering the role of the CC in HD is a novel concept. In agreement with our current results, recent transgenic mouse studies have found that callosal alterations can successfully discriminate mice with HD from those unaffected by HD pathology (Carroll et al. 2011).

Finally, in the literature (Kloppel et al. 2008; Tabrizi et al. 2009; Rosas et al. 2010), WM modifications have been related to some of the complex cognitive symptoms of HD, including symptoms that are less readily explained by invoking cortico-striatal dysfunction. Although we did not investigate this aspect here, we hypothesize that callosal aberrations may relate to some of the cognitive alterations typical of HD. For instance, the early changes we found in the isthmus (Schmahmann and Pandya 2006) may be associated with alterations in visuospatial and auditory functions generally evident in these patients (Kloppel et al. 2008; Saft et al. 2008).

Conclusion

Our data support the assumption of an early WM demyelination damage in HD. In addition, we suggest that the callosal damage progresses in a posterior–anterior direction. In the most advanced stages of the disease, the damage has spread considerably involving the entire CC body. Finally, we found that CC changes are related to changes of the cerebral cortex and to a measure of HD progression.

Our data suggest the CC to be a key neuropathological structure in the development of HD which may stimulate further research investigating the CC as a potential brain biomarker of HD. Given the cross-sectional nature of the current study, future longitudinal studies are needed to elucidate the pathogenic mechanisms related to the temporal sequence of the cerebral events (i.e., early WM demyelination vs. late axonal degeneration) and to other factors such as iron accumulation.

Funding

We are grateful for support from the Italian association of HD families "Associazione-Italiana-Corea-di-Huntington-Neuromed" (funds from 5 × 1000 to F.S. and F.E.), IRCCS Neuromed (institutional funds from 5 × 1000 to S.O.), Ministry of Health, Italy (Ricerca Corrente to F.S. and S.O.), the Italian Olympic Committee (CONI), and the European Huntington's Disease Network for the REGISTRY Study (to F.S., F.E., and S.O.).

Notes

Conflict of Interest : None declared.

References

Aboitiz F, Montiel J. 2003. One hundred million years of interhemispheric communication: the history of the corpus callosum. Braz J Med Biol Res. 36:409–420.

Aboitiz F, Scheibel AB, Fisher RS, Zaidel E. 1992. Fiber composition of the human corpus callosum. Brain Res. 598:143–153.

Adams JH, Graham DI. 1994. An introduction to neuropathology. Edinburgh (UK): Churchill Livingstone.

Ashburner J, Friston KJ. 2000. Voxel-based morphometry—the methods. Neuroimage. 11:805–821.

Bartzokis G, Lu PH, Tishler TA, Fong SM, Oluwadara B, Finn JP, Huang D, Bordelon Y, Mintz J, Perlman S. 2007. Myelin breakdown and iron changes in Huntington's disease: pathogenesis and treatment implications. Neurochem Res. 32:1655–1664.

Beal MF. 1996. Mitochondria, free radicals, and neurodegeneration. Curr Opin Neurobiol. 6:661–666.

Beaulieu C. 2002. The basis of anisotropic water diffusion in the nervous system—a technical review. NMR Biomed. 15:435–455.

Bechtel N, Scahill RI, Rosas HD, Acharya T, van den Bogaard SJ, Jauffret C, Say MJ, Sturrock A, Johnson H, Onorato CE, et al. 2010. Tapping linked to function and structure in premanifest and symptomatic Huntington disease. Neurology. 75:2150–2160.

Carroll JB, Lerch JP, Franciosi S, Spreeuw A, Bissada N, Henkelman RM, Hayden MR. 2011. Natural history of disease in the YAC128 mouse reveals a discrete signature of pathology in Huntington disease. Neurobiol Dis. 43:257–265.

Choi SJ, Lim KO, Monteiro I, Reisberg B. 2005. Diffusion tensor imaging of frontal white matter microstructure in early Alzheimer's disease: a preliminary study. J Geriatr Psychiatry Neurol. 18:12–19.

Ciarmiello A, Cannella M, Lastoria S, Simonelli M, Frati L, Rubinsztein DC, Squitieri F. 2006. Brain white-matter volume loss and glucose hypometabolism precede the clinical symptoms of Huntington's disease. J Nucl Med. 47:215–222.

Deichmann R, Schwarzbauer C, Turner R. 2004. Optimisation of the 3D MDEFT sequence for anatomical brain imaging: technical implications at 1.5 and 3 T. Neuroimage. 21:757–767.
Di Paola M, Di Iulio F, Cherubini A, Blundo C, Casini AR, Sancesario G, Passafiume D, Caltagirone C, Spalletta G. 2010. When, where and how corpus callosal changes in preclinical and clinical AD using multimodal MRI at 3 Tesla. Neurology. 74:1136–1142.
Di Paola M, Luders E, Di Iulio F, Varsi AE, Sancesario G, Passafiume D, Thompson PM, Caltagirone C, Toga AW, Spalletta G. 2010. Callosal atrophy in mild cognitive impairment and Alzheimer's disease: different effects in different stages. Neuroimage. 49:141–149.
Di Paola M, Spalletta G, Caltagirone C. 2010. In vivo structural neuroanatomy of corpus callosum in Alzheimer's disease and mild cognitive impairment using different MRI techniques: a review. J Alzheimers Dis. 20:67–95.
Douaud G, Gaura V, Ribeiro MJ, Lethimonnier F, Maroy R, Verny C, Krystkowiak P, Damier P, Bachoud-Levi AC, Hantraye P, et al. 2006. Distribution of grey matter atrophy in Huntington's disease patients: a combined ROI-based and voxel-based morphometric study. Neuroimage. 32:1562–1575.
Esmaeilzadeh M, Ciarmiello A, Squitieri F. 2011. Seeking brain biomarkers for preventive therapy in Huntington disease. CNS Neurosci Ther. 17:368–386.
Gomez-Tortosa E, MacDonald ME, Friend JC, Taylor SA, Weiler LJ, Cupples LA, Srinidhi J, Gusella JF, Bird ED, Vonsattel JP, et al. 2001. Quantitative neuropathological changes in presymptomatic Huntington's disease. Ann Neurol. 49:29–34.
Good CD, Johnsrude IS, Ashburner J, Henson RN, Friston KJ, Frackowiak RS. 2001. A voxel-based morphometric study of ageing in 465 normal adult human brains. Neuroimage. 14:21–36.
Hobbs NZ, Henley SM, Ridgway GR, Wild EJ, Barker RA, Scahill RI, Barnes J, Fox NC, Tabrizi SJ. 2010. The progression of regional atrophy in premanifest and early Huntington's disease: a longitudinal voxel-based morphometry study. J Neurol Neurosurg Psychiatry. 81:756–763.
Huntington's Disease Collaborative Research Group 1993. A novel gene containing a trinucleotide repeat that is expanded and unstable on Huntington's disease chromosomes. Cell. 72:971–983.
Huntington Study Group 1996. Unified Huntington's Disease Rating Scale: reliability and consistency. Mov Disord. 11:136–142.
Kassubek J, Juengling FD, Kioschies T, Henkel K, Karitzky J, Kramer B, Ecker D, Andrich J, Saft C, Kraus P, et al. 2004. Topography of cerebral atrophy in early Huntington's disease: a voxel based morphometric MRI study. J Neurol Neurosurg Psychiatry. 75:213–220.
Kim H, Piao Z, Liu P, Bingaman W, Diehl B. 2008. Secondary white matter degeneration of the corpus callosum in patients with intractable temporal lobe epilepsy: a diffusion tensor imaging study. Epilepsy Res. 81:136–142.
Kim JH, Budde MD, Liang HF, Klein RS, Russell JH, Cross AH, Song SK. 2006. Detecting axon damage in spinal cord from a mouse model of multiple sclerosis. Neurobiol Dis. 21:626–632.
Kloppel S, Draganski B, Golding CV, Chu C, Nagy Z, Cook PA, Hicks SL, Kennard C, Alexander DC, Parker GJ, et al. 2008. White matter connections reflect changes in voluntary-guided saccades in presymptomatic Huntington's disease. Brain. 131:196–204.
Kubicki M, Styner M, Bouix S, Gerig G, Markant D, Smith K, Kikinis R, McCarley RW, Shenton ME. 2008. Reduced interhemispheric connectivity in schizophrenia-tractography based segmentation of the corpus callosum. Schizophr Res. 106:125–131.
Langbehn DR, Brinkman RR, Falush D, Paulsen JS, Hayden MR. 2004. A new model for prediction of the age of onset and penetrance for Huntington's disease based on CAG length. Clin Genet. 65:267–277.
Leys D, Pruvo JP, Parent M, Vermersch P, Soetaert G, Steinling M, Delacourte A, Defossez A, Rapoport A, Clarisse J, et al. 1991. Could Wallerian degeneration contribute to "leuko-araiosis" in subjects free of any vascular disorder? J Neurol Neurosurg Psychiatry. 54:46–50.
Luders E, Di Paola M, Tomaiuolo F, Thompson PM, Toga AW, Vicari S, Petrides M, Caltagirone C. 2007. Callosal morphology in Williams syndrome: a new evaluation of shape and thickness. Neuroreport. 18:203–207.
Luders E, Narr KL, Bilder RM, Thompson PM, Szeszko PR, Hamilton L, Toga AW. 2007. Positive correlations between corpus callosum thickness and intelligence. Neuroimage. 37:1457–1464.
Luders E, Narr KL, Zaidel E, Thompson PM, Jancke L, Toga AW. 2006. Parasagittal asymmetries of the corpus callosum. Cereb Cortex. 16:346–354.
Mascalchi M, Lolli F, Della Nave R, Tessa C, Petralli R, Gavazzi C, Politi LS, Macucci M, Filippi M, Piacentini S. 2004. Huntington disease: volumetric, diffusion-weighted, and magnetization transfer MR imaging of brain. Radiology. 232:867–873.
Nichols TE, Holmes AP. 2002. Nonparametric permutation tests for functional neuroimaging: a primer with examples. Hum Brain Mapp. 15:1–25.
Nopoulos PC, Aylward EH, Ross CA, Johnson HJ, Magnotta VA, Juhl AR, Pierson RK, Mills J, Langbehn DR, Paulsen JS. 2010. Cerebral cortex structure in prodromal Huntington disease. Neurobiol Dis. 40:544–554.
Paulsen JS, Zhao H, Stout JC, Brinkman RR, Guttman M, Ross CA, Como P, Manning C, Hayden MR, Shoulson I. 2001. Clinical markers of early disease in persons near onset of Huntington's disease. Neurology. 57:658–662.
Penney JB, Vonsattel JP, MacDonald ME, Gusella JF, Myers RH. 1997. CAG repeat number governs the development rate of pathology in Huntington's disease. Ann Neurol. 41:689–692.
Pierpaoli C, Barnett A, Pajevic S, Chen R, Penix LR, Virta A, Basser P. 2001. Water diffusion changes in Wallerian degeneration and their dependence on white matter architecture. Neuroimage. 13:1174–1185.
Rosas HD, Hevelone ND, Zaleta AK, Greve DN, Salat DH, Fischl B. 2005. Regional cortical thinning in preclinical Huntington disease and its relationship to cognition. Neurology. 65:745–747.
Rosas HD, Koroshetz WJ, Chen YI, Skeuse C, Vangel M, Cudkowicz ME, Caplan K, Marek K, Seidman LJ, Makris N, et al. 2003. Evidence for more widespread cerebral pathology in early HD: an MRI-based morphometric analysis. Neurology. 60:1615–1620.
Rosas HD, Lee SY, Bender AC, Zaleta AK, Vangel M, Yu P, Fischl B, Pappu V, Onorato C, Cha JH, et al. 2010. Altered white matter microstructure in the corpus callosum in Huntington's disease: implications for cortical "disconnection". Neuroimage. 49:2995–3004.
Rosas HD, Liu AK, Hersch S, Glessner M, Ferrante RJ, Salat DH, van der Kouwe A, Jenkins BG, Dale AM, Fischl B. 2002. Regional and progressive thinning of the cortical ribbon in Huntington's disease. Neurology. 58:695–701.
Rosas HD, Salat DH, Lee SY, Zaleta AK, Pappu V, Fischl B, Greve D, Hevelone N, Hersch SM. 2008. Cerebral cortex and the clinical expression of Huntington's disease: complexity and heterogeneity. Brain. 131:1057–1068.
Rosas HD, Tuch DS, Hevelone ND, Zaleta AK, Vangel M, Hersch SM, Salat DH. 2006. Diffusion tensor imaging in presymptomatic and early Huntington's disease: selective white matter pathology and its relationship to clinical measures. Mov Disord. 21:1317–1325.
Saft C, Schuttke A, Beste C, Andrich J, Heindel W, Pfleiderer B. 2008. fMRI reveals altered auditory processing in manifest and premanifest Huntington's disease. Neuropsychologia. 46:1279–1289.
Schmahmann J, Pandya D. 2006. Fiber pathways of the brain. New York: Oxford University Press.
Schulte T, Sullivan EV, Muller-Oehring EM, Adalsteinsson E, Pfefferbaum A. 2005. Corpus callosal microstructural integrity influences interhemispheric processing: a diffusion tensor imaging study. Cereb Cortex. 15:1384–1392.
Sled JG, Zijdenbos AP, Evans AC. 1998. A nonparametric method for automatic correction of intensity nonuniformity in MRI data. IEEE Trans Med Imaging. 17:87–97.
Smith SM, Jenkinson M, Johansen-Berg H, Rueckert D, Nichols TE, Mackay CE, Watkins KE, Ciccarelli O, Cader MZ, Matthews PM, et al. 2006. Tract-based spatial statistics: voxelwise analysis of multi-subject diffusion data. Neuroimage. 31:1487–1505.
Song SK, Sun SW, Ju WK, Lin SJ, Cross AH, Neufeld AH. 2003. Diffusion tensor imaging detects and differentiates axon and myelin degeneration in mouse optic nerve after retinal ischemia. Neuroimage. 20:1714–1722.

Song SK, Sun SW, Ramsbottom MJ, Chang C, Russell J, Cross AH. 2002. Dysmyelination revealed through MRI as increased radial (but unchanged axial) diffusion of water. Neuroimage. 17:1429–1436.
Squitieri F, Gellera C, Cannella M, Mariotti C, Cislaghi G, Rubinsztein DC, Almqvist EW, Turner D, Bachoud-L vi AC, Simpson SA, et al. 2003. Homozygosity for CAG mutation in Huntington disease is associated with a more severe clinical course. Brain. 126:946–955.
Stoffers D, Sheldon S, Kuperman JM, Goldstein J, Corey-Bloom J, Aron AR. 2010. Contrasting gray and white matter changes in preclinical Huntington disease: an MRI study. Neurology. 74:1208–1216.
Sun SW, Song SK, Harms MP, Lin SJ, Holtzman DM, Merchant KM, Kotyk JJ. 2005. Detection of age-dependent brain injury in a mouse model of brain amyloidosis associated with Alzheimer's disease using magnetic resonance diffusion tensor imaging. Exp Neurol. 191:77–85.
Tabrizi SJ, Langbehn DR, Leavitt BR, Roos RA, Durr A, Craufurd D, Kennard C, Hicks SL, Fox NC, Scahill RI, et al. 2009. Biological and clinical manifestations of Huntington's disease in the longitudinal TRACK-HD study: cross-sectional analysis of baseline data. Lancet Neurol. 8:791–801.
Tomaiuolo F, Carlesimo GA, Di Paola M, Petrides M, Fera F, Bonanni R, Formisano R, Pasqualetti P, Caltagirone C. 2004. Gross morphology and morphometric sequelae in the hippocampus, fornix, and corpus callosum of patients with severe non-missile traumatic brain injury without macroscopically detectable lesions: a T1 weighted MRI study. J Neurol Neurosurg Psychiatry. 75:1314–1322.
Vonsattel JP, DiFiglia M. 1998. Huntington disease. J Neuropathol Exp Neurol. 57:369–384.
Walker FO. 2007. Huntington's disease. Lancet. 369:218–228.
Weaver KE, Richards TL, Liang O, Laurino MY, Samii A, Aylward EH. 2009. Longitudinal diffusion tensor imaging in Huntington's Disease. Exp Neurol. 216:525–529.
Yassa MA, Stark CE. 2009. A quantitative evaluation of cross-participant registration techniques for MRI studies of the medial temporal lobe. Neuroimage. 44:319–327.